

Coupled Experimental and Computational Approach for CABRI Power Transients Analysis

Olivier Clamens^{ID}, Patrick Blaise^{ID}, Jean-Pascal Hudelot^{ID}, Johann Lecerf, Bertrand Duc, Laurent Pantera, and Bruno Biard

Abstract—CABRI is an experimental pulse reactor, funded by the French Nuclear Safety and Radioprotection Institute and operated by Commissariat à l’Énergie Atomique et aux Énergies Alternatives at the Cadarache Research Center. It is designed to study fuel behavior under reactivity-initiated accident conditions. In order to produce the power transients, reactivity is injected by depressurization of a neutron absorber (^3He) situated in the so-called transient rods inside the reactor core. The CABRI reactivity injection system allows us to generate structured transients based on specific sequences of depressurization. For such transients, the time difference between the openings of two valves of the reactivity injection system has an important impact on the power pulse shape. A kinetic point code, SPARTE, was developed in order to replace the older DULCINEE code dedicated to the modeling and prediction of CABRI power transients. The SPARTE code includes new models of ^3He depressurization based on CFD calculations, variable Doppler coefficient based on Monte Carlo calculations, and variable axial neutron flux profile. The density and Doppler models have a large impact on power transient prediction. For low initial pressure transients, the major uncertainty comes from the reactivity injected by the ^3He depressurization. For high initial pressure transients, the ^3He heating during the power pulse (“TOP effect”) is responsible of an additional injection of reactivity that needs to be modeled precisely.

Index Terms—CABRI, multiphysics, power transients, SPARTE.

I. INTRODUCTION

CABRI is an experimental pulse reactor funded by the French Nuclear Safety and Radioprotection Institute (IRSN) and operated by Commissariat à l’Énergie Atomique et aux Énergies Alternatives (CEA) at the Cadarache Research Center. Since 1978 [1]–[3], the experimental programs have been aiming at studying the fuel behavior under reactivity-initiated accident (RIA) conditions. In order to study the PWR high burn-up fuel behavior under such transients, the facility was modified to accept a pressurized

Manuscript received September 29, 2017; revised May 29, 2018; accepted June 11, 2018. Date of publication June 14, 2018; date of current version September 14, 2018.

O. Clamens, P. Blaise, J.-P. Hudelot, J. Lecerf, B. Duc, and L. Pantera are with DEN CAD/DER/SPESI—Commissariat à l’Énergie Atomique et aux Énergies Alternatives Cadarache, 13108 Saint-Paul-Lez-Durance, France (e-mail: olivier.clamens@cea.fr).

B. Biard is with IRSN/PSN-RES/SEREX Cadarache, 13115 Saint-Paul-Lez-Durance Cedex, France.

Color versions of one or more of the figures in this paper are available online at <http://ieeexplore.ieee.org>.

Digital Object Identifier 10.1109/TNS.2018.2847331

water loop in its central part, able to reproduce thermal hydraulics characteristics representative of PWR nominal operating conditions (155 bar, 300 °C). This project, which began in 2003 and supported first commissioning tests from October 2015 to March 2017, was driven within a broader scope including both an overall facility refurbishment and a complete safety review [4] (stability to earthquakes, for example). The global modifications have been conducted by the CEA project team and funded by IRSN, which is operating and managing the CIP [5] experimental program (CABRI International Program), in the framework of an OECD/NEA agreement. The CIP program will investigate several UO_x and MOX LWR spent fuel samples under RIA conditions, with a foreseen completion by the end of 2023. Power transients are generated by a dedicated so-called transient rods system [6] allowing the very fast depressurization of ^3He tubes positioned inside the CABRI core.

The calculation of power transients of the RIA type, in any reactor is a multiphysics problem. Fast calculation can be performed on normal computers thanks to simplified multiphysics including 1-D thermal hydraulics and heat transfers and point kinetics [7], [8]. Nowadays, the DULCINEE [9] code, based on those principles, can be run for CABRI power transient calculations. The philosophy of this paper is to add physical models based on the best-estimate calculations and experimental analysis to the point kinetic in order to improve the calculation precision.

The first part of this paper is dedicated to the description of the CABRI power transients. In the second part, we will address the prediction of those transients and speak about the models that were added to the newly developed SPARTE code in order to improve the prediction precision. This paper also focuses on experimental and calculation uncertainties and their impact on the CABRI power transients.

II. CABRI POWER TRANSIENTS

The CABRI power transients are generated by the depressurization of pressurized ^3He contained in the transients rods located at the four corners of the core (see Fig. 1). The transient rods system is composed of 96 tubes spread around four fuel assemblies linked to a system of control and fast opening valves constituting a low and a high flow rate channels (see Fig. 2). The initial transient state is obtained by the withdrawal of the control and safety rods to the critical position.

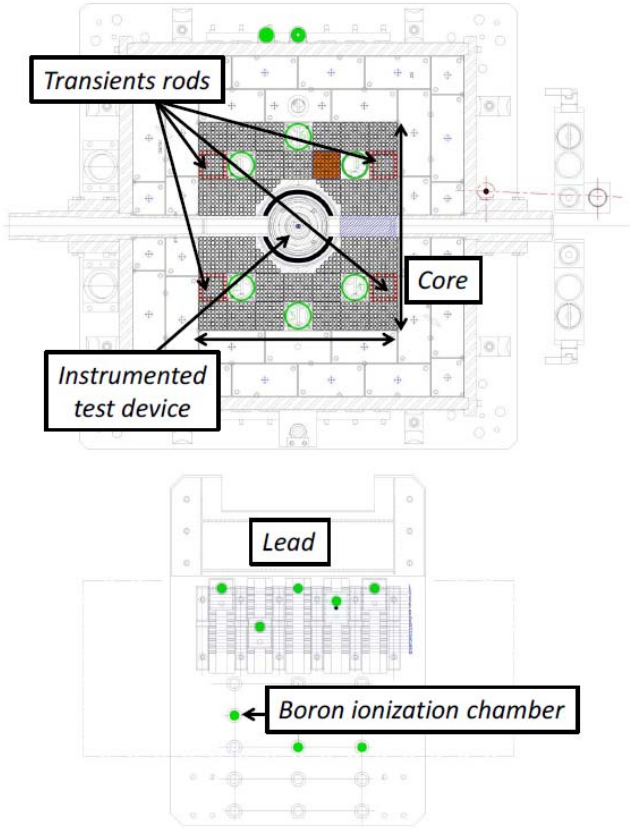


Fig. 1. Experimental boron ionization chambers near CABRI core.

A. Transients Measurement

Two types of transients are needed for the CIP program. First ones are natural transients described in the following paragraph. Second ones are structured transients described in the next paragraph.

Specific boron-lined ionization chambers are used for measuring high power levels during steady states or during power transients [?]. In the case of power transients, several boron ionization chambers, located at increasing distances from the core (see Fig. 1), are used to cover the whole power range (i.e., from 100 kW to \sim 20 GW). More details can be found in [4], [11], and [12].

B. Natural Transients

Natural transients consist of single pulses with a full-width at half-maximum (FWHM) of approximately 10 ms. They are made by single opening of the high flow rate channel (VABT01, see Fig. 2).

One example of natural transient is reproduced in Fig. 3. The reactivity injected by ${}^3\text{He}$ depressurization causes a power increase. The energy deposited in the fuel leads to a temperature increase. When the injected reactivity is balanced by Doppler and other reactivity feedbacks, the power decreases until a new equilibrium is reached. The reaction is then completely stopped by dropping the control rods. The parameters of the experiment are the control valve aperture

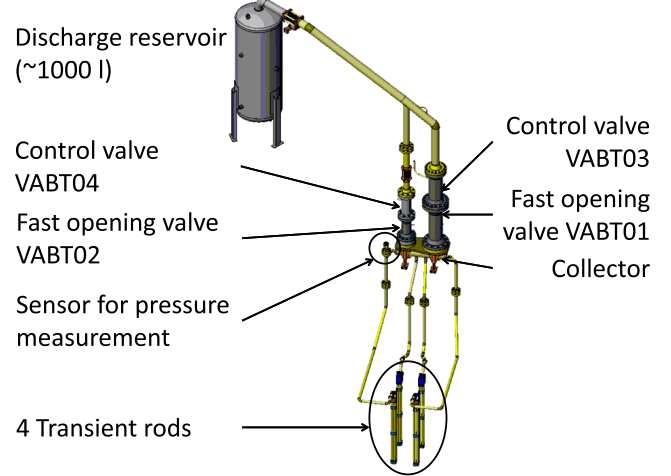


Fig. 2. Main components of the CABRI transient rods.

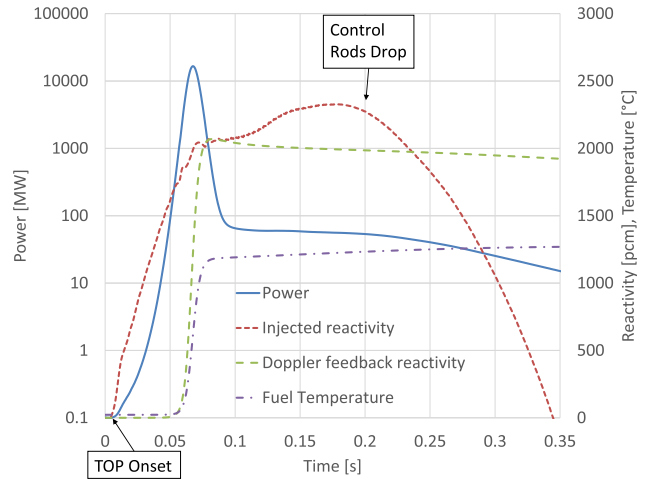


Fig. 3. Natural power transient and reactivity analysis.

(VABT03), the initial ${}^3\text{He}$ pressure, the rod drop instant, the initial stabilized power, and the initial system temperature. The transient shape is mostly depending on the valve aperture and the initial pressure. The energy deposited in the core during the power transient is also controlled by the rod drop instant. The initial temperature is really important, in order to know the exact ${}^3\text{He}$ quantity in transient rods.

C. Structured Transient

In order to be a representative of other RIA conditions of nuclear power plants, it is necessary to be able to increase the FWHM of the transient. This can be done by opening successively the fast opening valves of the low and then of the high flow-rate channels. When the net reactivity is close to 1\$, the high flow rate channel is opened to compensate during a short instant the reactivity feedbacks by a fast reactivity insertion. It allows thus a more important energy deposit during the pulse. The adjustment of the time difference between the openings of the fast opening valves allows us

to generate so-called structured transients characterized by FWHM varying from 20 to 80 ms.

III. IMPACT OF TIMING FOR STRUCTURED TRANSIENTS

The experimentalists issue is to generate, with the CABRI core, the ideal power transient for the experimental purposes. One goal of the reactor commissioning tests performed in the first 2017 quarter was to generate power transients with an FWHM of 30 ms with a sufficient energy deposit. This can be achieved with structured transients as described in the last paragraph. In order to reach experimental goals, the transient parameters have to be precisely mastered. Considering an initial power of 100 kW, the different parameters are:

- 1) the apertures of the two control valves (VABT03 and VABT04);
- 2) the ${}^3\text{He}$ initial pressure;
- 3) the opening time of the two fast opening valves (VABT01 and VABT02).

A. Timing Issue

The uncertainties on the initial pressure and the valve apertures are small ($\sigma \simeq 1\%$). However, an uncertainty exists on the time needed for the fast valves to open. A standard deviation of approximately 2 ms was observed on the opening time of VABT01. A major improvement was carried out during the CABRI renovation in order to reduce and master the uncertainty linked to the VABT02 opening. In the past, the second valve opening signal was triggered when pressure reached 90% of its initial value. The limitation of this method is that at the beginning of the depressurization, many oscillations are recorded. Those variations are linked to the different ${}^3\text{He}$ flows coming from different locations of the circuit. Those variations are reproducible from a depressurization to another and can also be observed in detailed CFD calculations. A few milliseconds of uncertainty were then added to the standard deviation observed for VABT01. The opening command of the second valve is now given by the specific control device when pressure reaches 75% of its initial value. In that zone, no variations are observed, only 0.25 ms of uncertainty can be added due to the acquisition rate. In Fig. 4, we can observe the time gap between the two openings of the high flow rate channels on two “structured” transients that have the same parameters. This gap is under 1 ms, but still has a real impact on the transient shape.

B. Impact on Power Transients

The difference between the two power transients is depicted in Fig. 5. The two peaks climax at the same moment. However, the maximum powers (1-GW gap) and FWHM (6-ms gap) are different. When the opening time comes faster, the power is going higher and the transient is a little thinner. Nevertheless, the total deposited energy difference is around 1 MJ on a total of 200. Before every irradiated fuel test, a campaign of approximately 10 transients without test rod in the central cell is performed. For a transient with a nominal value of 30-ms FWHM, a dispersion from -5 to $+5$ ms on FWHM can be observed.

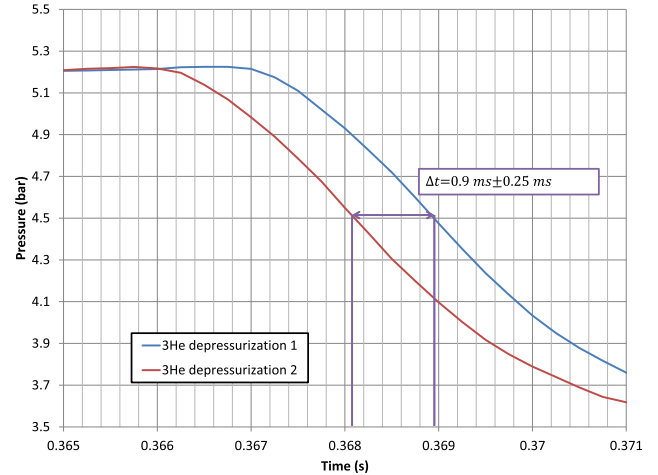


Fig. 4. Difference between two VABT01 opening times on two commissioning tests under the same conditions.

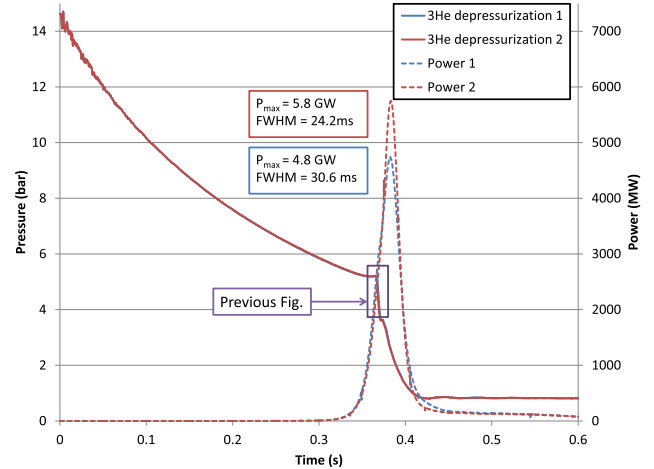


Fig. 5. Comparison of the two power transients resulting from the two similar depressurizations.

IV. SPARTE, A POINT KINETICS CODE DESIGNED FOR CABRI

In order to analyze and to predict the CABRI power transients, some code runs are performed before each test as follows.

- 1) The DULCINEE code is used to compute the power transient shape thanks to point kinetics, core thermal hydraulics, and heat transfers.
- 2) The SCANAIR [12] code is used to compute the hotter fuel thermal-mechanical behavior for safety application.

A new code is being developed in order to improve the prediction capacity as for kinetics aspects. The goal of this code is to improve the prediction of the CABRI power transients in terms of reached maximal power, FWHM, energy deposited and timing of the peaks.

SPARTE (see Fig. 6) is a new code adapted to CABRI transients. It is based on the DULCINEE point kinetics code.

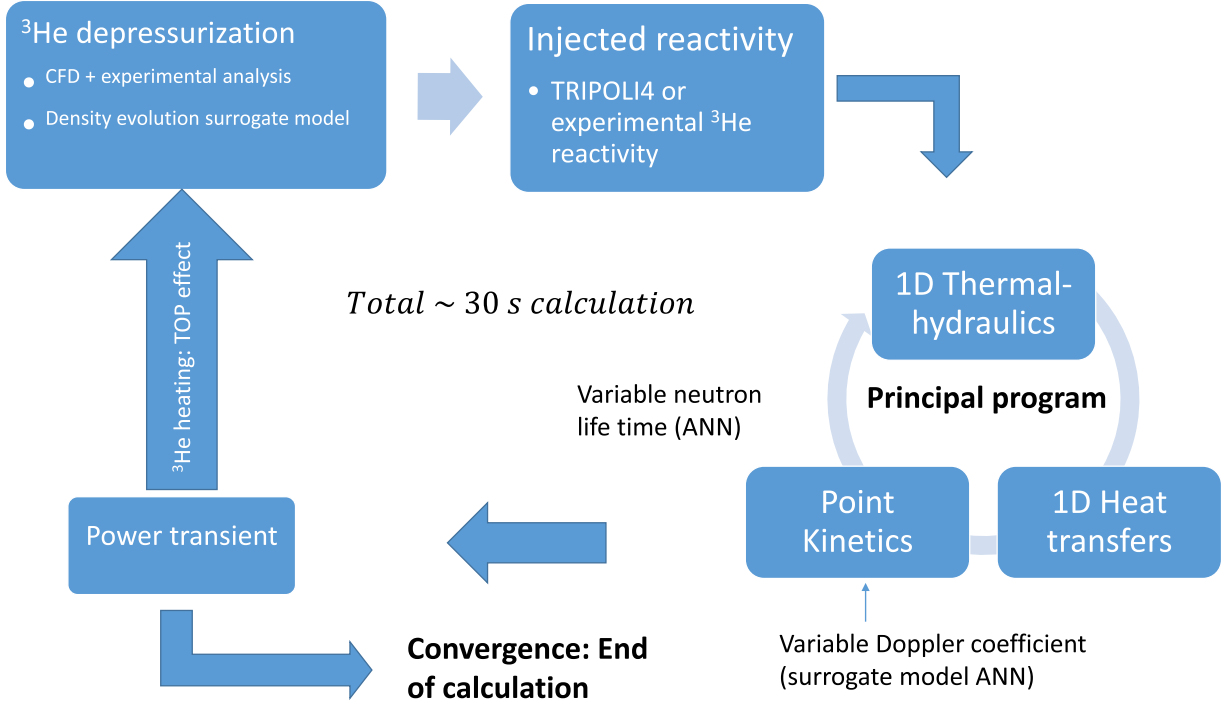


Fig. 6. SPARTE code—CABRI power transient solving.

Surrogate models and modifications of the datasets have been added in order to be more representative of the physical conditions. Surrogate models are based on the best-estimate calculations (CFD [13] and Monte Carlo [14]) and built with artificial neuronal networks with URANIE [15]. In this section, we will present the four main improvements and their impacts on the transient prediction:

- 1) surrogate model of the ³He density in transient rods during depressurization;
- 2) variability of the Doppler coefficient as a function of the transient of power conditions;
- 3) axial neutron flux profile depending on the control rods position;
- 4) variability of the prompt neutron lifetime during power transients;
- 5) modeling the ³He transient heating impact on the gas depressurization (TOP effect).

In every section, improvements will be added one by one on an example of transient. This example is a “natural” transient based on a depressurization beginning at 7 bar of ³He with a full aperture of the high flow rate channel. It is a very fast transient impacted by the different models added into SPARTE.

A. Surrogate Model of Helium Density Evolution

CFD calculations have been made in order to evaluate the ³He density in the transient rods volume. A surrogate model estimating the ³He density in the transient rods has thus been developed and implemented [13]. The ³He density in the transient rods is more relevant than the ³He pressure measured by the sensors (see Fig. 2) to take into account the impact of the ³He temperature in the reactivity injection calculation. This

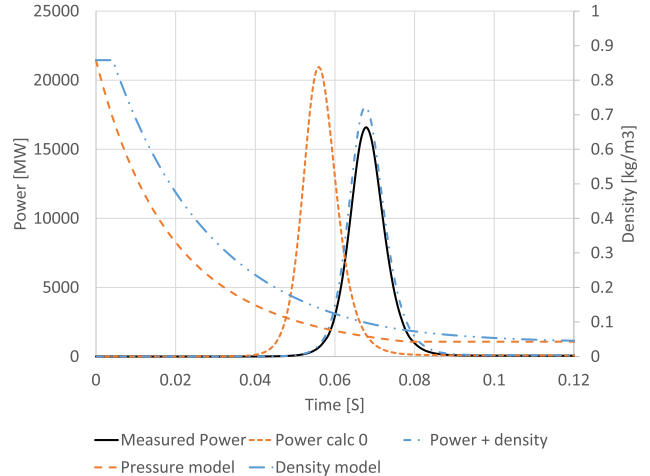


Fig. 7. Effect of density model on the power transient calculation.

model replaces the old model based on the analytical solution of the ³He depressurization (demonstration in [16]):

$$P(t) = P_0 \left(\frac{m(t)}{m_0} \right)^\gamma = P_0 [Bt + 1]^{\frac{-2\gamma}{\gamma - 1}} \quad (1)$$

where P is the ³He pressure, m is the ³He mass inside the transient rods, B is a characteristic inverse time linked to the system volume and temperature and to the valve cross section, and γ is the heat capacities ratio.

Fig. 7 represents the difference between the density evolution and the pressure evolution. We can see that the pressure evolution is much faster than the density evolution. Therefore, the reactivity injection calculated with the pressure curve is

also much faster. That is why, the real power transient comes after the power transient calculated with the pressure model. The density model has a big effect on the transient shape and needs to be added to the code.

B. Variability of the Doppler Coefficient

Neutronics calculations of the CABRI core using the French stochastic TRIPOLI4 [14] code show that the Doppler coefficient is varying with CABRI power transients conditions. The Doppler coefficient varies with fuel temperature and core poisoning due to ${}^3\text{He}$ and to control rods. This can be explained by the hardness of neutron spectrum. The ${}^3\text{He}$ neutron absorption is very effective under thermal condition. The more the ${}^3\text{He}$ pressure in the transient rods important is, the harder the neutron spectrum. The hardness of the neutron spectrum is also increasing with the elevation of the fuel temperature.

An artificial neuronal network was created using the results of TRIPOLI4 simulations of the CABRI core. The parameters of the surrogate model are:

- 1) the elevation “z” of the control rods (Hafnium);
- 2) the density “d” of ${}^3\text{He}$ is the transient rods;
- 3) the fuel temperature “T” (UO_2).

700 simulations were completed based on Latin hypercube sampling. The resulting surrogate model computes the multiplication factor depending on different parameters. In SPARTE, the Doppler coefficient is on the integral form and is defined as follows:

$$\rho_D = A_D * (\sqrt{T} - \sqrt{T_0}). \quad (2)$$

We can also write the Doppler reactivity depending on the multiplication factor k as follows:

$$\rho_D = \rho(T) = \rho(z, d, T) - \rho(z, d, T_0) \quad (3)$$

where

$$\rho = \frac{k - 1}{k}. \quad (4)$$

From (2)–(4), we can deduce (5)

$$A_D = \frac{\frac{k(z, d, T) - 1}{k(z, d, T)} - \frac{k(z, d, T_0) - 1}{k(z, d, T_0)}}{\sqrt{T} - \sqrt{T_0}}. \quad (5)$$

Fig. 8 shows the evolution of the Doppler coefficient with temperature at different ${}^3\text{He}$ pressures in the transient rods, the control rod insertion being fixed. The Doppler coefficient increases in an absolute value with fuel temperature and a core poison quantity. Thus, during a transient, the Doppler coefficient decreases because of the ${}^3\text{He}$ depressurization, and in the same time increases because of the fuel temperature elevation. In the SPARTE code, the Doppler coefficient is then calculated as in (5), using the surrogate model of a multiplication factor. The Doppler coefficient is calculated at each time step and for each fuel mesh (r, z) as the temperature.

Fig. 9 represents the influence of the Doppler coefficient model added to the SPARTE code. We can observe that the Doppler reactivity feedback is increasing higher with the

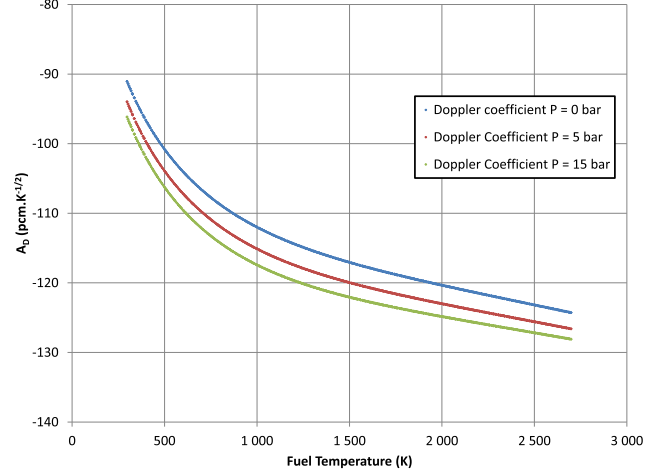


Fig. 8. Variability of the integral Doppler coefficient in CABRI core depending on fuel temperature and ${}^3\text{He}$ density.

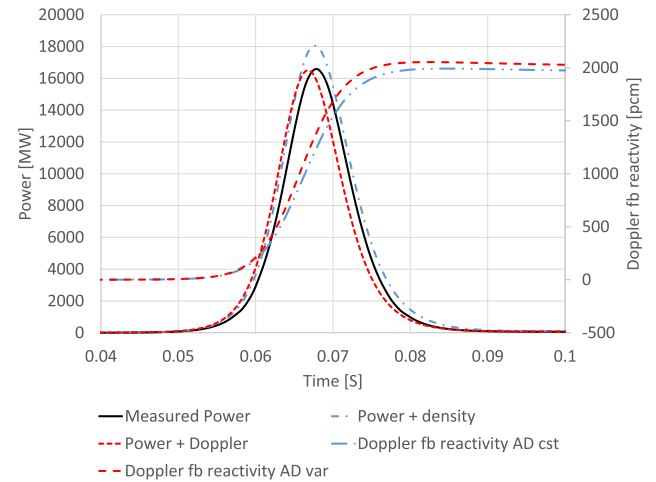


Fig. 9. Effect of Doppler model on the power transient calculation.

model than for a constant value of the Doppler coefficient. It is due to an elevation of the absolute value of the coefficient with increasing temperature. The addition of the Doppler surrogate model in the simulation reduces the FWHM of the calculated power transients.

C. Axial Neutron Flux Distribution

The axial neutron flux distribution is taken into account in the SPARTE code. It is used to calculate the energy deposition depending on the height of the fuel. It is also used to evaluate the axial distribution of the reactivity feedbacks (Doppler, void, and temperature). The CABRI case is specific because of the reactivity injection system. The control rods insertion, constant before triggering the depressurization and during the resulting pulse, until a manual scram order is initiated, depends at the first order on the initial ${}^3\text{He}$ density in the transient rods. Its dependency on the core cooling water temperature is secondary. That is why the axial profile needs to be calculated for every control rods axial position. Before the recent TRIPOLI4 calculation, the axial power

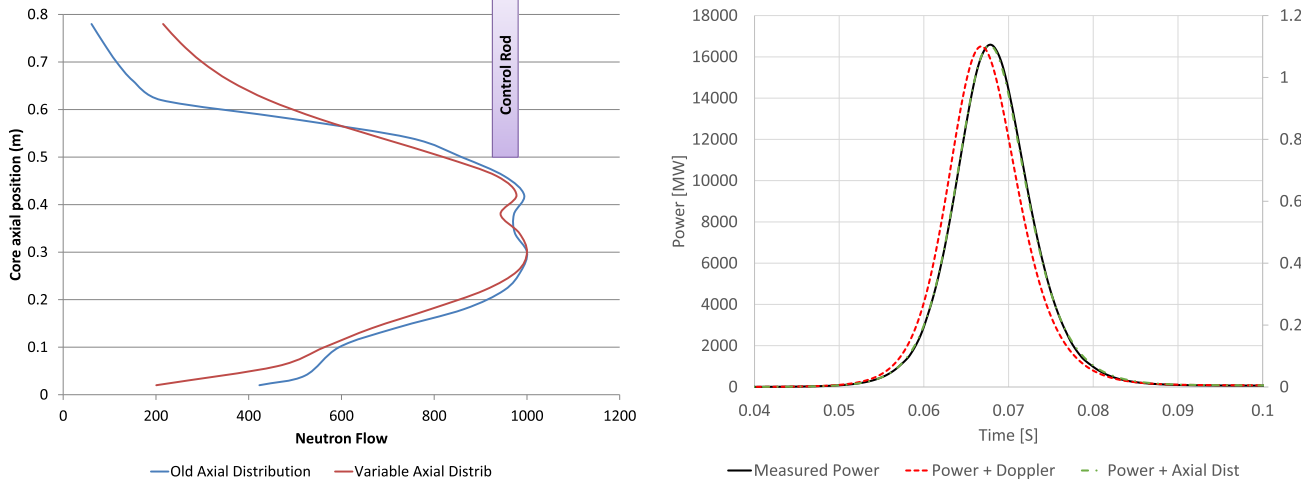


Fig. 10. Effect of axial distribution on the power transient calculation.

profile in DULCINEE was coming from calculations of the hot channel near the control rods. The axial power distribution was therefore too low on the top of the core in the old axial profile (see Fig. 10). In the SPARTE code, a surrogate model based on the TRIPOLI4 calculations was added to calculate the core averaged axial power profile depending on the control rods insertion.

We can see that in this case, the new axial distribution has a moderate influence on the power transient shape. The axial neutron flux distribution is flatter, so that the temperature is better distributed. The Doppler reactivity feedback is then a little higher. This reduces slightly the maximum power (see Fig. 10).

D. Variability of Neutron Lifetime

The CABRI transients are characterized by a rapid withdrawal of the ${}^3\text{He}$ neutron absorbers, uniform within the core volume. We can easily assume that this withdrawal is responsible of an extension of the neutron lifetime due to the withdrawal of a neutron absorber. TRIPOLI4 is able to calculate kinetics parameters [effective neutron mean generation time (critical neutron lifetime) “ Λ_{eff} ” and effective delayed neutron fraction “ β_{eff} ”] thanks to the iterated fission probability method [17]. The calculations demonstrate the variability of the neutron lifetime. The most influent parameter is the ${}^3\text{He}$ density. The second one is the control rods insertion.

The impact of the neutrons lifetime is presented in Fig. 11. We can observe that the neutrons lifetime is increasing with depressurization of the ${}^3\text{He}$. The neutrons lifetime being lower than the reference at the beginning of the transient, the power peak arises shortly before the previous calculation. However, the neutrons’ lifetime staying close to the reference and the impact on the transient calculation are low.

E. TOP Effect Model Based on Experiments and CFD

The SPARTE’s last improvement consists of modeling the TOP effect. This effect is detailed in [13]. The TOP effect comes from ${}^3\text{He}$ heating during power transients. As power

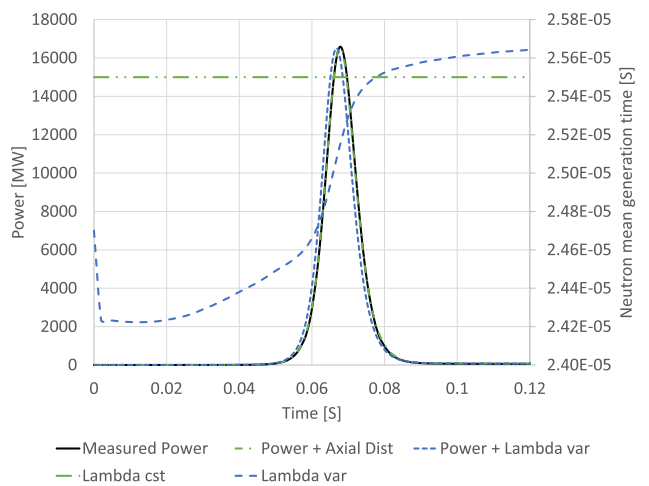


Fig. 11. Effect of neutron lifetime variability on the power transient calculation.

increases, the thermal neutron flux also increases. Therefore, the neutron absorption intensifies by ${}^3\text{He}$. This reaction produces two charged particles: proton and tritium. One part of their energies is deposited in the ${}^3\text{He}$ gas by ionization before reaching the metallic wall of the transient rods. The denser the gas, the higher the probability of ionization and more important the deposited energy is. The direct effect of this energy deposit is that the gas temperature increases more than 200 K when the ${}^3\text{He}$ pressure is still high (more than 2 bar) at the peak instant. A temperature increase is equivalent to a pressure increase. The differential pressure between rods and flow channels implies a faster depressurization of helium from the transient rods. This finally implies a rise of the reactivity injection speed. A surrogate model computing a deviation of the depressurization rate during power increasing was added to the code.

The impact of the TOP effect is presented in Fig. 12. As we can see, the TOP effect model brings a deviation to the density evolution curve during the transient.

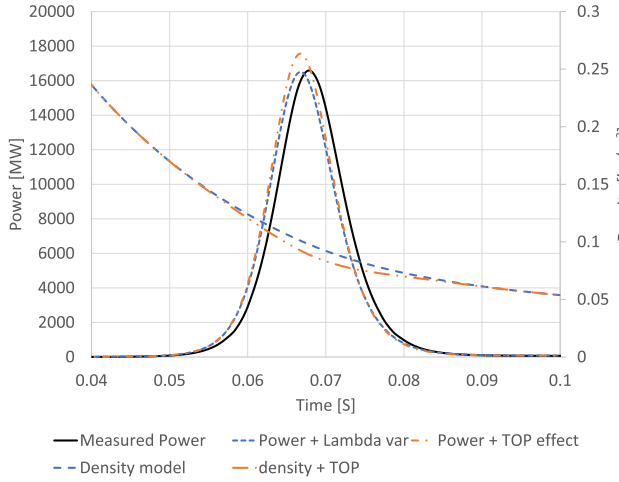


Fig. 12. Impact of the TOP effect model on the power transient calculation.

The supplementary reactivity inserted through the TOP effect completes the prediction of the transient.

F. Comparative Tables

In this paragraph, the successive elaborated models are tested on different power transients. Four criteria are compared to the experiment:

- 1) the maximum power “ P_{max} ” of the transient;
- 2) the FWHM of the pulse;
- 3) the energy “ E ” deposited in the core after 1.2 s;
- 4) the instant of the peak “ t_{peak} .”

All the transients compared are performed by single opening of a channel. Tables I–IV show the four chosen examples:

- 1) a transient with low initial pressure (1.3 bar) and the maximum aperture of VABT03 (high flow rate channel) (Table I);
- 2) a transient with a middle initial pressure (4 bar) and a low aperture of VABT04 (low flow rate channel) (Table II);
- 3) a transient with a relatively high initial pressure (7 bar) and the maximum aperture of VABT03 (Table III);
- 4) a transient with the maximal initial pressure (~ 14.5 bar) and a low aperture of VABT04 (Table IV).

For the four cases, the same approach is used. First, the measurement is presented. Then, a calculation shows the result of SPARTE with four models presented deactivated. The different models previously presented are then added one by one to the calculation. The last line of each table corresponds to the calculated power transient with all models activated.

We can observe that in all cases, the density evolution model and the Doppler coefficient model are the most influent on transient calculations. The density model brings the calculated peak closer to the measured peak in the time. The Doppler coefficient is higher than the reference in cases of high power (Table III), the calculated power being then lower. In all the cases, the Doppler model has for effect to reduce the FWHM. It is due to the elevation of the fuel temperature during the

TABLE I
LOW INITIAL PRESSURE (1.3 BAR) TRANSIENT

Models	P_{max} (MW)	FWHM (ms)	E (MJ)	t_{peak} (ms)
Measurement	127	89.9	16.9	201
Calc 0	262	65.1	26.3	162
+ density	251	67.7	25.6	182
+ Doppler	252	66.3	25.2	182
+ Ax dist	243	66.3	24.4	181
+ Λ_{eff}	243	66.3	24.4	181
+ TOP	243	66.3	24.4	181

TABLE II
MIDDLE INITIAL PRESSURE (4 BAR) TRANSIENT

Models	P_{max} (MW)	FWHM (ms)	E (MJ)	t_{peak} (ms)
Measurement	546	48.4	56	436
Calc 0	647	47.3	84.8	376
+ density	635	48.2	83.2	404
+ Doppler	629	46.5	77.3	403
+ Ax dist	613	46.5	76.1	403
+ Λ_{eff}	611	45.9	76.3	400
+ TOP	596	46.2	76.3	400

TABLE III
RELATIVELY HIGH INITIAL PRESSURE (7 BAR) TRANSIENT

Models	P_{max} (MW)	FWHM (ms)	E (MJ)	t_{peak} (ms)
Measurement	16600	9.57	197	67.7
Calc 0	20900	9.58	247	55.9
+ density	18000	10.2	228	67.7
+ Doppler	16500	9.60	197	66.7
+ Ax dist	16600	9.66	198	67.7
+ Λ_{eff}	16500	9.60	197	66.7
+ TOP	17600	9.41	204	66.7

TABLE IV
VERY HIGH INITIAL PRESSURE (14.5 BAR) TRANSIENT

Models	P_{max} (MW)	FWHM (ms)	E (MJ)	t_{peak} (ms)
Measurement	3400	24.1	108	376
Calc 0	1080	37.0	92.0	340
+ density	1050	37.7	84.4	367
+ Doppler	1020	36.4	78.1	366
+ Ax dist	1040	36.2	79.3	366
+ Λ_{eff}	1030	35.3	79.6	363
+ TOP	4200	20.5	116	371

power increase, which influences the Doppler coefficient by elevating it. The Doppler reactivity feedback is then higher and the power reduces faster.

Table IV shows the importance of the TOP effect modeling on the maximum power and the total deposited energy determination. We can observe that the other models bring capabilities to improve the power transient timing modeling. But some reactivity effects are missing and are then brought by the TOP effect.

We can also observe that for the low initial pressure transient (Table I) calculations are a bit far from reality. We will

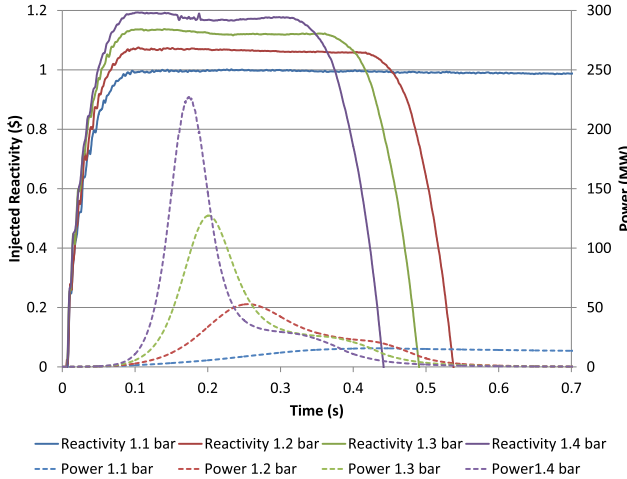


Fig. 13. Effect of small initial pressure variations on measured power transients.

demonstrate in Section V that this gap can be explained by the uncertainty on pressure and on conversion from pressure to reactivity.

V. SENSITIVITY STUDY NEAR 1\$ OF INJECTED REACTIVITY

In this section, we will try to explain the differential between calculation and experiment for low initial pressure transients, based on an uncertainty propagation approach. There is an uncertainty on the pressure measurement of approximately 0.2% and an uncertainty on ${}^3\text{He}$ reactivity versus ${}^3\text{He}$ density. In the cases of low pressure and an injected reactivity close to the effective delayed neutron fraction, the uncertainties are very influent on transient calculation.

A. Experimental Approach

During the last commissioning tests, some transients have been carried out with an initial pressure close to 1.2 bar in order to observe the changing physics in this zone. We will compare four transients with close initial pressure (1.1, 1.2, 1.3, and 1.4 bar).

We can observe those transients in Fig 13. Below 1\$ of injected reactivity, no power pulse is observed, and the power increases slower but continues to increase before the rod drop. Above the dollar of injected reactivity, power is increasing until the Doppler feedback compensates the injected reactivity.

B. Computational Approach

The computational approach consists in propagating the input uncertainties on the power transient calculation. We assume uncertainties on initial pressure, final density, helium reactivity curve, Doppler coefficient model, and depressurization model. Those uncertainties are assumed with a standard deviation of around 5%. 40 code runs are launched using a Design of experiments based on the Sobol sequences [18] with normal distribution of the input parameters. These sequences

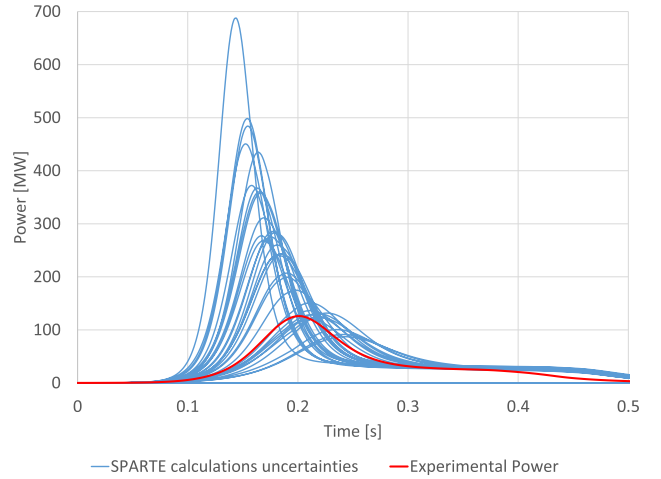


Fig. 14. Uncertainty propagation on the 1.3-bar case with the SPARTE code launched by URANIE.

use a base of two to form successively finer uniform partitions of the unit interval and then reorder the coordinates in each dimension. The computational approach is tested on the 1.3-bar initial pressure case.

We can observe in Fig. 14 the influence of small uncertainties on the calculated transient of power. In this area of the reactivity curve function of the ${}^3\text{He}$ pressure, we can assume that the reactivity model overestimates the reality. The experimental power transient (red) is located near the lower limit of the calculated transients. A good consistency is observed between the experiment and calculation when uncertainties are taken into account.

VI. CONCLUSION

The CABRI power transients generated by ${}^3\text{He}$ controlled depressurization are of two types: “natural” and “structured” and present very complex behavior depending on the kinetics and feedback coefficients. The current DULCINEE multi-physics code, while conservative, presents several assumptions that must be upgraded to enhance safety and operational margins of the CABRI tests. The first goal of the new SPARTE code is to predict at best the “natural” transients. The implementation of surrogate models for the ${}^3\text{He}$ density, more relevant than the pressure, for the Doppler coefficient, the axial neutron flux distribution and the neutron lifetime, based on the best-estimate calculation and validated against measurements has greatly improved the calculation of those transients. For the prediction of the “structured” transients, we need first to calculate with a good consistency the transients issued from depressurizations of the low flow rate channel. When the initial pressure is under 5 bar, SPARTE reproduces quite well the measured transients. Over this pressure, the “TOP” effect (described in [13]) affects the reactivity injection speed. We finally observed that the calculation of power transients with injected reactivity near 1\$ is very sensible to different uncertainties. The analysis of the CABRI commissioning tests recently performed will improve the precision of the reactivity injected by the ${}^3\text{He}$ depressurization.

APPENDIX A
NOMENCLATURE

Name	Definition
P	Pressure.
m	Mass.
B	Coefficient in s^{-1} used in depressurization analytical law.
γ	Heat capacity ratio.
ρ	Reactivity.
ρ_D	Doppler reactivity.
A_D	Doppler integral coefficient.
T	Absolute temperature.
T_0	Initial absolute temperature.
k	Multiplication factor.
z	Height of insertion of control rods.
d	^3He density.

REFERENCES

- [1] G. Kussmaul, W. Vaeth, J. Wolff, J. Dadillon, M. Haessler, and F. Sabathier, "The CABRI project—Overall status and achievements," in *Proc. Int. Conf. Sci. Technol. Fast Reactor Saf.* London, U.K.: BNES, 1986, pp. 103–108.
- [2] I. Sato, F. Lemoine, and D. Struwe, "Transient fuel behavior and failure condition in the CABRI-2 experiments," *Nucl. Technol.*, vol. 145, no. 1, pp. 115–137, 2004. [Online]. Available: http://inis.iaea.org/Search/search.aspx?orig_q=RN:38013454
- [3] J. Papin *et al.*, "Summary and interpretation of the CABRI REP-Na program," *Nucl. Technol.*, vol. 157, no. 3, pp. 230–250, Mar. 2007. [Online]. Available: <http://epubs.ans.org/?a=3815>
- [4] J.-P. Hudelot *et al.*, "CABRI facility: Upgrade, refurbishment, recommissioning and experimental capacities," in *Proc. Int. Conf. PHYSOR*, Sun Valley, ID, USA, 2016, pp. 2286–2298.
- [5] *CABRI CIP Program*. Accessed: May 25, 2018. [Online]. Available: <http://www.irsn.fr/en/research/research-organisation/research-programmes/cabri-international-program/pages/cabri-cip-program.aspx>
- [6] B. Duc, B. Biard, P. Debias, L. Pantera, J.-P. Hudelot, and F. Rodiac, "Renovation, improvement and experimental validation of the Helium-3 transient rods system for the reactivity injection in the CABRI reactor," in *Proc. Int. Group Res. Reactors (IGORR)*, Bariloche, Argentina, Nov. 2014.
- [7] N. H. Badrun, M. H. Altaf, M. A. Motalab, M. S. Mahmood, and M. J. H. Khan, "Modeling of SPERT IV reactivity initiated transient tests in EUREKA-2/RR code," *Int. J. Nucl. Energy*, vol. 2014, 2014, Art. no. 167426, doi: [10.1155/2014/167426](https://doi.org/10.1155/2014/167426).
- [8] S. Chatzidakis, A. Ikonomopoulos, and S. E. Day, "PARET-ANL modeling of a SPERT-IV experiment under different departure from nucleate boiling correlations," *Nucl. Technol.*, vol. 177, no. 1, pp. 119–131, Jan. 2012. [Online]. Available: <http://pubs.ans.org/?a=13332>
- [9] G. Ritter, R. Berre, and L. Pantera, "DULCINEE. Beyond neutron kinetics, a powerful analysis software," in *Proc. RRFM IGORR*, Prague, Czech Republic, Mar. 2012.
- [10] J. Lecerf, Y. Garnier, J. Hudelot, B. Duc, and L. Pantera, "Study of the linearity of CABRI experimental ionization chambers during RIA transients," in *Proc. EPJ Web Conf.*, vol. 170, 2018, p. 04015. [Online]. Available: https://articles/epjconf/abs/2018/05/epjconf_animma2018_04015/epjconf_animma2018_04015.html
- [11] J. P. Hudelot *et al.*, "A complete dosimetry experimental program in support of the core characterization and of the power calibration of the CABRI reactor," in *Proc. 4th Int. Conf. Adv. Nucl. Instrum. Meas. Methods Appl. (ANIMMA)*, Apr. 2015, pp. 1–8. [Online]. Available: <http://ieeexplore.ieee.org/abstract/document/7465504/>
- [12] V. Georgenthum, A. Moal, and O. Marchand, "SCANAIR a transient fuel performance code Part two: Assessment of modelling capabilities," *Nucl. Eng. Des.*, vol. 280, pp. 172–180, Dec. 2014. [Online]. Available: <http://www.sciencedirect.com/science/article/pii/S0029549314002556>
- [13] O. Clamens, J. Lecerf, J.-P. Hudelot, B. Duc, P. Blaise, and B. Biard, "Modeling of the ^3He density evolution inside the CABRI transient rods during power transients," *IEEE Trans. Nucl. Sci.*, to be published, doi: [10.1109/TNS.2018.2818928](https://doi.org/10.1109/TNS.2018.2818928).
- [14] E. Brun *et al.*, "TRIPOLI-4, CEA, EDF and AREVA reference Monte Carlo code," *Ann. Nucl. Energy*, vol. 82, pp. 151–160, Aug. 2015. [Online]. Available: <http://www.sciencedirect.com/science/article/pii/S0306454914003843>
- [15] F. Gaudier, "URANIE: The CEA/DEN uncertainty and sensitivity platform," *Procedia-Social Behavioral Sci.*, vol. 2, no. 6, pp. 7660–7661, Jan. 2010. [Online]. Available: <http://www.sciencedirect.com/science/article/pii/S1877042810013078>
- [16] O. Clamens, J. Lecerf, B. Duc, J.-P. Hudelot, T. Cadiou, and B. Biard, "Assessment of the CABRI transients power shape by using CFD and point kinetic codes," in *Proc. Int. Conf. PHYSOR*, Sun Valley, ID, USA, 2016, pp. 1747–1758.
- [17] G. Truchet, P. Leconte, A. Santamarina, E. Brun, F. Damian, and A. Zolia, "Computing adjoint-weighted kinetics parameters in Tripoli-4 by the iterated fission probability method," *Ann. Nucl. Energy*, vol. 85, pp. 17–26, Nov. 2015. [Online]. Available: <http://www.sciencedirect.com/science/article/pii/S030645491500225X>
- [18] I. M. Sobol', "On the distribution of points in a cube and the approximate evaluation of integrals," *USSR Comput. Math. Math. Phys.*, vol. 7, no. 4, pp. 86–112, Jan. 1967. [Online]. Available: <http://www.sciencedirect.com/science/article/pii/0041555367901449>